

Showcasing research from Professor Alexander Solovev and Professor Yongfeng Mei's laboratories, Department of Materials Science, Fudan University, Shanghai, China.

Carbon dioxide bubble-propelled microengines in carbonated water and beverages

The generation of carbon dioxide microbubbles is observed from rolled-up tubular nanomembranes in carbonated water and brewed beverages. When released from the substrate, buoyant microtubes operate as microengines with well-controlled vertical position, angle of rotation and buoyancy.

As featured in:



See Gaoshan Huang,  
Alexander A. Solovev *et al.*,  
*Chem. Commun.*, 2018, 54, 5692.



[rsc.li/chemcomm](http://rsc.li/chemcomm)

Registered charity number: 207890



# Carbon dioxide bubble-propelled microengines in carbonated water and beverages†

Yan Zhang, Hong Zhu, Wenxuan Qiu, Yilu Zhou, Gaoshan Huang, \*  
 Yongfeng Mei  and Alexander A. Solovev \*

Cite this: *Chem. Commun.*, 2018, 54, 5692

Received 5th February 2018,  
 Accepted 27th March 2018

DOI: 10.1039/c8cc01011k

rsc.li/chemcomm

**We demonstrate a new type of gaseous fuel for rolled-up tubular Ti/Cr microengine powered by carbon dioxide microbubbles in carbonated water and brewed beverages. Existence of microbubble pockets is revealed using on-chip integrated transparent microtubes. Vertical position, angle of rotation and buoyancy of ferromagnetic Ti/Fe/Cr microengines are controlled using an external magnetic field.**

Autonomous nano-/micro-motors and engines<sup>1–6</sup> show multiple potential applications including drug delivery,<sup>7,8</sup> biosensing in motion<sup>9</sup> and environmental remediation.<sup>10</sup> Bubble-propelled tubular microengines have several advantages including high speed, motive power and efficiency.<sup>3,11–13</sup> It is a common belief that the realization of alternative fuels is the next important prerequisite for further advancement in biomedical applications of nano/micromotors.<sup>14</sup> Emerging materials for fabrication and applications of micromotors have recently been considered by the groups of Escarpa<sup>15</sup> and Pumera.<sup>16,17</sup> Fuel-free motion, such as ultrasound<sup>18</sup> and magnetic field<sup>19</sup> driven micro-/nanomotors, are demonstrated. Alternatively, enzymes such as catalase, urease, or glucose oxidase (upon addition of corresponding substrates: H<sub>2</sub>O<sub>2</sub>, urea and glucose),<sup>20</sup> and reactions between magnesium–water<sup>21</sup> and aluminum alloy–water<sup>22</sup> have been identified as promising approaches to power micromotors. However, a number of important limitations should be taken into account. For instance, for an operation of microengines *in vivo*, both fuels and reaction products must be a part of the metabolic pathways or cellular respiration. Carbon dioxide (CO<sub>2</sub>) is a well-known organic compound required for photosynthesis and in beverage industries and thus is one of the most feasible gaseous fuels for micromachines. Recently, Schmidt's group demonstrated motion of calcium carbonate Janus particles in ultra-light acidic environment generated by cancer cells according to the reaction: CaCO<sub>3</sub> + 2H<sup>+</sup> → Ca<sup>2+</sup> + CO<sub>2</sub> + H<sub>2</sub>O.<sup>23</sup> Still, carbonate

micromotors have a limited lifetime, resulting in dissolution within a couple of minutes. In another study, Wang's group demonstrated rapid CO<sub>2</sub> sequestration by hydrogen peroxide-driven micromotors.<sup>24</sup> Pumera and co-workers achieved acetylene bubble-powered capsules driven by the reaction of calcium carbide with water as a co-reactant.<sup>25</sup> Nucleation and generation of bubbles bring forth fundamental interests in research, and the utilization of the unique bubble properties at the micro- and nano-scale such as stability, lifetime, contraction, dissolution, growth, coalescence, cavitation, surface charge, surface area, flexibility/rigidity of air-gas interface, internal pressure, buoyancy, growth and mass transfer rates.<sup>26</sup> Micro- and nanobubbles are used for ultrasound biomedical imaging, cleaning of rivers and lakes, water purification, froth flotation, additives to fuels and oil reservoirs, *etc.* In contrast to homogeneous nucleation in liquid, heterogeneous bubble nucleation on solid surfaces reduces the energy barrier required for bubble nucleation. In addition, stored bubble pockets or stable gas embryos can lower the energy barrier required for stable generation of bubbles. For instance, pouring of carbonated water and brewed beverages leads to stable nucleation, expansion, growth and generation of bubbles from the pre-existing gas pockets entrapped in the surface defects, crevices, pits or cavities.<sup>27</sup> The subsequent growth and generation of bubbles depends strongly on the size of surface imperfections, wetting properties of the surface, diffusion of molecules and gas saturation in a liquid. According to Jones, Evans and Galvin, if pre-existing gas cavities can house menisci with radii of curvature greater than the critical nucleation value, they provide a stable source for bubble nucleation.<sup>28</sup> Several examples of bubble nucleation are reported in small capillary tubes<sup>29</sup> and cellulose fibers,<sup>30</sup> resembling Taylor-like bubbles trapped in microchannels. In cellulose fiber, the gas pocket remains entrapped inside the microtube, where it grows and generates bubbles at stable rates.<sup>31,32</sup> Usually, the size of bubbles can be controlled by external pressure,<sup>33</sup> CO<sub>2</sub> dissolution rate,<sup>34</sup> liquid temperature<sup>35</sup> and hydrophobicity of the surface.<sup>36</sup>

Herein, we report a new type of CO<sub>2</sub> fuel for bubble-propelled microengines consisting of rolled-up Ti/Cr, Ti/Fe/Cr and SiO/SiO<sub>2</sub> nanomembranes. Our previous method of strain-engineered

Department of Materials Science, Fudan University, 220 Handan Rd, Shanghai, P. R. China. E-mail: gshuang@fudan.edu.cn, solovevlab@gmail.com

† Electronic supplementary information (ESI) available. See DOI: 10.1039/c8cc01011k

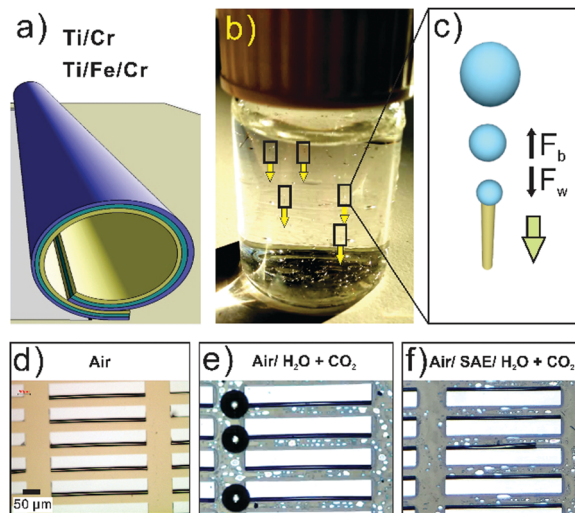


**Fig. 1** Motion of microtubes in carbonated water and on-chip study of bubble generation conditions (sample S1). (a) A schematic of microtubes consisting of rolled-up metallic nanomembranes. (b) Optical image of experimental observation of buoyant microtubes' vertical movement self-aligned under gravity in carbonated water. (c) A schematic image of forces acting on an individual microtube:  $F_b$  (buoyancy force of bubble),  $F_w$  (weight of tube). (d) Optical microscopy image of an array of rolled-up microtubes located in air. (e) The same sample was immersed in carbonated water, where growing  $\text{CO}_2$  bubbles are observed from tubular openings. (f) The same sample after treatment in water solution with added common soap, acetone and ethanol (in separate beakers), followed by final positioning in carbonated water solution.

nanomembranes on polymers was used to fabricate microtubes with well-controlled wall thickness, diameter, length and a number of rotations.<sup>4</sup> Herein, we tested several samples (S1: Ti/Cr tubes on photoresist; S2: Ti/Cr, Ti/Fe/Cr on table salt; S3: SiO/SiO<sub>2</sub> on photoresist) using a fabrication procedure described elsewhere.<sup>4</sup> Fig. 1(a–c) shows a schematic of a rolled-up microtube and the experimental observation of microtubes self-propelled in a vertical direction. Fig. 1(d–f) indicates optical microscopy images of rolled-up Ti/Cr microtubes located in air and different solutions. For observing bubble nucleation and growth, we placed our dried sample with integrated rolled-up Ti/Cr tubes in air (Fig. 1(d)), followed by the sample transfer to carbonated water (Fig. 1(e)). Clear growth of  $\text{CO}_2$  bubbles was observed from tubular openings. Next, our sample was immersed in water solution with added surfactants (common soap),<sup>37</sup> acetone and ethanol (in three separate beakers, indicated as SAE treatment), followed by transfer to carbonated water containing freshly added  $\text{CO}_2$ . Bubble generation from the rolled-up microtubes was suppressed (Fig. 1(f)). This finding suggested the existence of gas pockets in the microtubes, which were subsequently removed by our sample treatment method in different solutions.

Fig. 2 shows growth of microbubbles in carbonated water, where microbubbles are generated from rolled-up Ti/Cr microtubes. Initially, the rolled-up microtubes were integrated on Si substrate and placed in a Petri dish, and  $\text{CO}_2$  was subsequently added (Fig. 2(a)). The growth and contraction of an individual bubble are illustrated in a schematic image (Fig. 2(b)). Optical microscopy image sequences, shown in Fig. 2(c),  $t_1$ – $t_4$ , indicated growth of bubbles

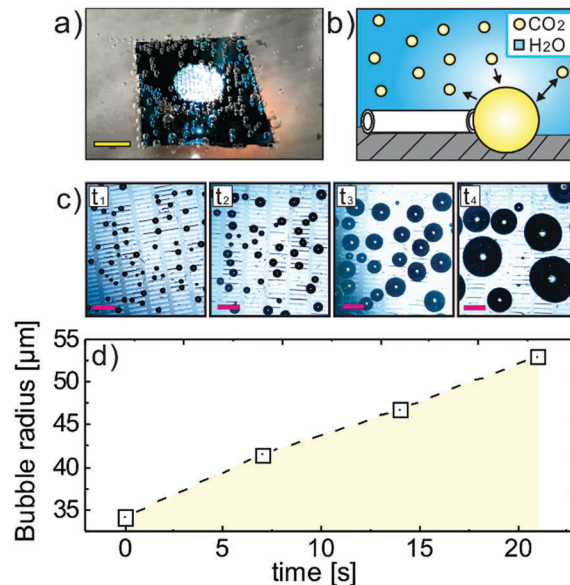


**Fig. 2** The growth of  $\text{CO}_2$  bubbles from Ti/Cr microtubes integrated on Si surface (sample S1). (a) A sample with rolled-up microtubes was placed in a Petri dish with added carbonated water. Scale bar 5 mm. (b) A schematic image of an individual rolled-up microtube with a growing bubble. (c) Optical microscopy image sequences of rapid growth and coalescence of bubbles from an array of rolled-up Ti/Cr microtubes. Scale bar 400  $\mu\text{m}$ . (d) Increase of average bubble radius in time (for average, 20 bubbles were taken for each data point, Video 1, ESI†).

from an array of microtubes. A linear trend of bubble radius growth in time was observed where during 20 s, the average bubble radius increased from 34 to 53  $\mu\text{m}$  (see Video 1, ESI†). This observation corresponded with a general trend of linear increase of bubble diameter with respect to time under convection conditions.<sup>38</sup> Coalescence of neighbouring microbubbles was observed for bubbles growing in carbonated DI water. On the other hand, microbubbles rapidly contract if the solution was unsaturated with carbon dioxide due to a mass transfer rate from bubbles to liquid and high pressure in the microbubbles.

According to the Young–Laplace equation, homogeneous nucleation of bubbles in the liquid bulk depends strongly on the surface tension ( $\Delta P = 4\sigma/d$ ), where  $\Delta P$  is the bubble pressure,  $\sigma$  is the surface tension of a liquid and  $d$  is the diameter of the bubble.<sup>39</sup> Next, we tested the dependence of bubble detachment size on the concentration of surfactants (common soap)<sup>37</sup> in carbonated water. Surfactants are well-known to reduce surface tension, and they also stabilize small bubbles. Fig. 3(a) illustrates optical microscopy image sequences of microtubes in different concentrations of common soap  $c_1$  (0%; pure  $\text{CO}_2$  water),  $c_2$  (1% v/v) and  $c_3$  (10% v/v). The radius of generated bubbles was strongly reduced from an average value of 105  $\mu\text{m}$  (0%, DI  $\text{CO}_2$  water) to 75  $\mu\text{m}$  (1% v/v soap,  $\text{CO}_2$  water, Video 2, ESI†) and 16  $\mu\text{m}$  (10% v/v soap,  $\text{CO}_2$  water, Video 3, ESI†).

Microparticles with low weights are known to self-propel and produce bubbles in carbonated water and beverages. However, previously, speed and buoyancy of microparticles could not be precisely controlled due to variable microparticle weights. The rolled-up tubular nanomembranes (*i.e.*, microengines) are based on a desirable number of layers' rotation, precisely controlled layer

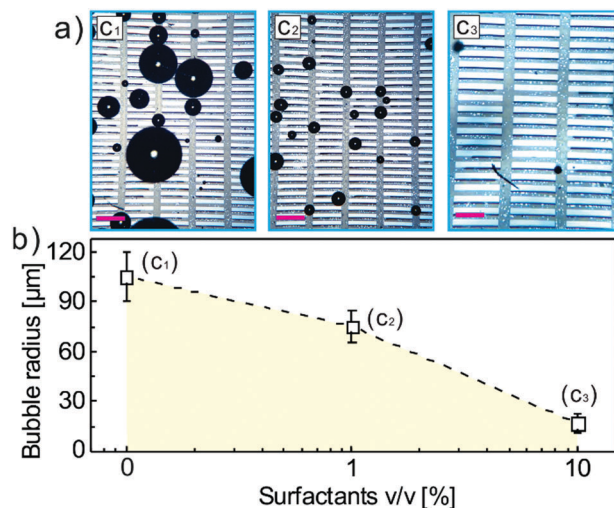


Fig. 3 Pre-tests of Ti/Cr microengines integrated on-chip in different concentrations of surfactants (sample S1). (a) Optical microscopy images indicating CO<sub>2</sub> bubble detachment radius controlled by surfactants (common soap) in carbonated water: c<sub>1</sub> (0%, DI CO<sub>2</sub> water), c<sub>2</sub> (1% v/v, CO<sub>2</sub> water) and c<sub>3</sub> (10% v/v, CO<sub>2</sub> water). Scale bar 400  $\mu\text{m}$ . (b) Bubble detachment radius as a function of surfactant concentration.

thickness, length, weight and buoyancy in solution. In addition, if a ferromagnetic layer is incorporated, the rolled-up microtubes can be rotated and the buoyancy force can be controlled by accumulation of gas in the tubular microcavity. Fig. 4 shows the self-propelled motion of an individual microtube and the control of its vertical position (buoyancy) using an external magnetic field. An average downward velocity of  $-82.3 \mu\text{m s}^{-1}$  is detected at  $0^\circ$  angle, whereas a tube rotation to  $90^\circ$  leads to an average upward velocity of  $251.2 \mu\text{m s}^{-1}$  due to an increased buoyancy force within seconds.

If tubular nanomembrane buoyancy is neglected, the balance of forces can be simplified to  $F_b = F_w$ , where  $F_b$  is the buoyancy of the bubble and  $F_w$  is the weight of the tube. Considering our experimental observation where microtubes remain neutrally buoyant for minutes, the bubble radius required for a neutral buoyancy of microengines can be estimated using the following equation:

$$R_B = \sqrt[3]{3abL\rho_T/4\pi\rho_1} \quad (1)$$

Here,  $\rho_1$  is the liquid density,  $\rho_T = \rho_{\text{Cr}} + \rho_{\text{Fe}} + \rho_{\text{Ti}}$  is the density of materials,  $g$  is acceleration due to gravity, and  $a$ ,  $b$ , and  $L$  are the width, thickness and length of the nanomembrane, respectively. In our case, the weight of the rolled-up tube (layer thickness Ti/Fe/Cr 20/5/20 nm, width = 50  $\mu\text{m}$ , length = 800  $\mu\text{m}$ ) is estimated to be 93.4 pN (Video 4, ESI†). Subsequently, CO<sub>2</sub> microbubbles with diameters as small as 20  $\mu\text{m}$  are sufficient to balance the weight and keep microengines in a neutrally buoyant position as is described by eqn (1). In time, the carbon dioxide concentration decreases and the bubble frequency also decreases, which slowly settles down the microtubes. It is important to note that we have previously demonstrated the same tubular geometry for catalytic microtubes driven by chemical decomposition of hydrogen peroxide, which were able to self-propel in all directions due to an

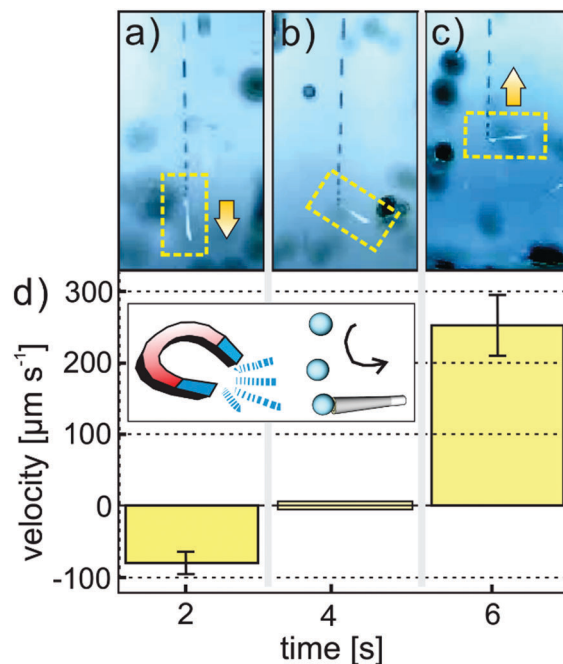
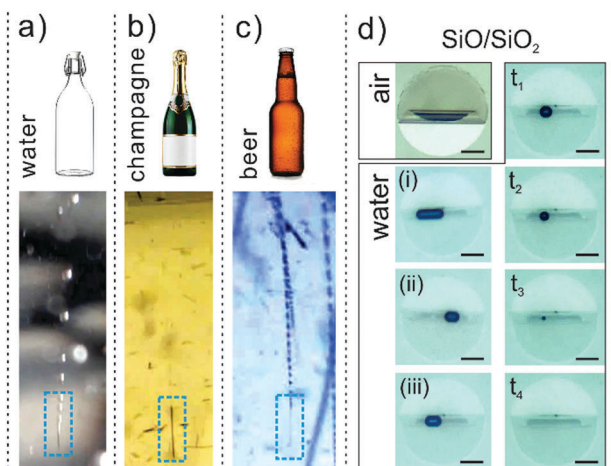


Fig. 4 Magnetic control of individual ferromagnetic Ti/Fe/Cr microtube (sample S2). (a) Slow sedimentation of microtube in carbonated water was observed. (b) Graph shows external magnetic control to rotate the microtube to  $90^\circ$ , which changes its weight-buoyancy ratio while keeping an average bubble frequency 16 Hz invariant with respect to the angle of rotation ( $0-90^\circ$ ). Arrow bars in (a–c) indicate the direction of the microtube motion. (d) The velocity of the microtube is changed within seconds when the tube is rotated using magnetic field. The inset image shows a schematic of the microtube external control. The external magnet was kept at a further distance to allow microtube rotation and avoid magnetic attraction (Video 4, ESI†).

efficient bubble-induced pumping mechanism.<sup>3,40</sup> In contrast, as is shown herein, CO<sub>2</sub>-powered microtubes do not self-propel in a horizontal direction, *i.e.*, perpendicular to gravity (Fig. 4). We hypothesize that the trapped gas pockets in rolled-up microtubes do not allow fluid pumping through tubes. This presumably accounts for the motion mechanism of the gaseous CO<sub>2</sub>-powered microengine differing from that of the catalytic H<sub>2</sub>O<sub>2</sub>-powered microengine.

Carbon dioxide is a widely used gas in the beverage industry, and it provides a unique approach for powering and testing microengines in various chemical conditions. We tested the motion of Ti/Cr microengines in commercially available sparkling water, beer and champagne as shown in Fig. 5(a–c) and Videos 5–7, ESI† To prove our hypothesis about the existence of gas pockets in microtubes, we fabricated transparent rolled-up SiO/SiO<sub>2</sub> dried tubes consisting of nanomembranes (sample S3), Fig. 5(d). Air gas pockets with different sizes and positions trapped inside microtubes when the sample was immersed in DI water (Fig. 5(d), (i–iii)). Moreover, if the sample was left in water without the addition of CO<sub>2</sub>, the gas pockets dissolved in minutes (Fig. 5(d),  $t_1-t_4$ , Video 8, ESI†). This indicated that an immediate addition of a carbon dioxide-containing gaseous fuel is required to activate the generation of bubbles and keep the gas pockets stable. We have reserved future research on effects of surface hydrophobicity, surface roughness,



**Fig. 5** Motion of Ti/Cr microtubes in commercially available beverages (sample S2): (a) carbonated water (Video 5, ESI†), (b) champagne (Video 6, ESI†) and (c) beer (Video 7, ESI†). These microtubes were fabricated using a water soluble NaCl sacrificial layer. (d) Tested transparent SiO/SiO<sub>2</sub> (sample S3) microtubes in water with added 1% v/v common soap. Gas pockets are clearly observed in microtubes. Optical microscopy images of different microtubes (i–iii) and dissolution/contraction of an individual gas pocket inside the transparent microtube ( $t_1 = 0$ ,  $t_2 = 5$  s,  $t_3 = 15$  s,  $t_4 = 16$  s). Scale bar 25  $\mu$ m.

tubular length, number of rotations and biocompatibility of microengines for potential *in vivo* and *in vitro* applications. In summary, a gaseous fuel based on CO<sub>2</sub> microbubbles can be a compelling alternative to power microengines. CO<sub>2</sub> is an active molecule in the biological metabolic pathways, which can be released from aqueous solutions and microbubbles to power microengines. Furthermore, rolled-up nanomembranes can provide new insights on nucleation, stability and generation of bubbles in microtubular cavities. It is noteworthy to mention that one important industrial application of the controllable buoyancy of microparticles includes separation and extraction of minerals from their ores by buoyant bubbles.

The authors would like to thank Dr Udit Choudhury and Prof. Peer Fischer for early assistance with experiments and fruitful discussions. AAS is deeply grateful for the 1000 Talents Plan grant. The authors gratefully acknowledge financial support from the Natural Science Foundation of China (grant no. 51475093).

## Conflicts of interest

Authors declare no conflict of interests.

## References

- W. F. Paxton, K. C. Kistler, C. C. Olmeda, A. Sen, S. K. S. Angelo, Y. Cao, T. E. Mallouk, P. E. Lammert and V. H. Crespi, *J. Am. Chem. Soc.*, 2004, **126**, 13424–13431.
- G. A. Ozin, I. Manners, S. Fournier-Bidoz and A. Arsenault, *Adv. Mater.*, 2005, **17**, 3011–3018.
- A. A. Solovev, Y. F. Mei, E. Bermudez Urena, G. S. Huang and O. G. Schmidt, *Small*, 2009, **5**, 1688–1692.
- Y. Mei, G. Huang, A. A. Solovev, E. Bermudez Urena, I. Moench, F. Ding, T. Reindl, R. K. Y. Fu, P. K. Chu and O. G. Schmidt, *Adv. Mater.*, 2008, **20**, 4085–4090.

- G. Huang, J. Wang, Z. Liu, D. Zhou, L. Li and Y. Mei, *Nanoscale*, 2017, **9**, 18590–18596.
- J. Li, I. Rozen and J. Wang, *ACS Nano*, 2016, **10**, 5619–5634.
- D. Patra, S. Sengupta, W. Duan, H. Zhang, R. Pavlick and A. Sen, *Nanoscale*, 2013, **5**, 1273–1283.
- Y. Tu, F. Peng, A. A. M. Andre, Y. Men, M. Srinivas and D. A. Wilson, *ACS Nano*, 2017, **11**, 1957–1963.
- B. Esteban-Fernández de Ávila, A. Martín, F. Soto, M. A. Lopez-Ramirez, S. Campuzano, G. M. Vázquez-Machado, W. Gao, L. Zhang and J. Wang, *ACS Nano*, 2015, **9**, 6756–6764.
- M. Safdar, J. Simmchen and J. Jänis, *Environ. Sci.: Nano*, 2017, **4**, 1602–1616.
- L. Liu, T. Bai, Q. Chi, Z. Wang, S. Xu, Q. Liu and Q. Wang, *Micromachines*, 2017, **8**, 267, DOI: 10.3390/mi8090267.
- J. Li, W. Liu, J. Wang, I. Rozen, S. He, C. Chen, H. G. Kim, H.-J. Lee, H.-B.-R. Lee, S.-H. Kwon, T. Li, L. Li, J. Wang and Y. Mei, *Adv. Funct. Mater.*, 2017, **27**, 1700598, DOI: 10.1002/adfm.201700598.
- B. Xu, B. Zhang, L. Wang, G. Huang and Y. Mei, *Adv. Funct. Mater.*, 2018, DOI: 10.1002/adfm.201705872.
- E. L. Chng, G. Zhao and M. Pumera, *Nanoscale*, 2014, **6**, 2119–2124.
- B. Jurado-Sánchez, M. Pacheco, R. Maria-Hormigos and A. Escarpa, *Appl. Mater. Today*, 2017, **9**, 407–418.
- H. Wang and M. Pumera, *Nanoscale*, 2017, **9**, 2109–2116.
- H. Wang and M. Pumera, *Chem. Rev.*, 2015, **115**, 8704–8735.
- T. Xu, L.-P. Xu and X. Zhang, *Appl. Mater. Today*, 2017, **9**, 493–503.
- X.-Z. Chen, M. Hoop, F. Mushtaq, E. Siringil, C. Hu, B. J. Nelson and S. Pané, *Appl. Mater. Today*, 2017, **9**, 37–48.
- X. Ma, A. C. Hortelão, T. Patiño and S. Sánchez, *ACS Nano*, 2016, **10**, 9111–9122.
- F. Mou, C. Chen, H. Ma, Y. Yin, Q. Wu and J. Guan, *Angew. Chem., Int. Ed.*, 2013, **125**, 7349–7353.
- W. Gao, A. Pei and J. Wang, *ACS Nano*, 2012, **6**, 8432–8438.
- M. Guix, A. K. Meyer, B. Koch and O. G. Schmidt, *Sci. Rep.*, 2016, **6**, 21701.
- M. Uygun, V. V. Singh, K. Kaufmann, D. A. Uygun, S. D. de Oliveira and J. Wang, *Angew. Chem., Int. Ed. Engl.*, 2015, **54**, 12900–12904.
- J. G. S. Moo, H. Wang and M. Pumera, *Chem. Commun.*, 2014, **50**, 15849–15851.
- H. Tsuge, *Micro- and Nanobubbles: Fundamentals and Applications*, Pan Stanford Publishing Pte. Ltd, 1st edn, 2014, ISBN 978-981-4463-10-2.
- Y. Xue, P. Lv, Y. Liu, Y. Shi, H. Lin and H. Duan, *Phys. Fluids*, 2015, **27**, 092003.
- S. F. Jones, G. M. Evans and K. P. Galvin, *Adv. Colloid Interface Sci.*, 1999, **80**, 27–50.
- G. J. Brereton, R. J. Crilly and J. R. Spears, *Chem. Phys.*, 1998, **230**, 253–265.
- C. Voisin, P. Jeandet and G. Liger-Belair, *Colloids Surf., A*, 2005, **263**, 303–314.
- G. Liger-Belair, C. Voisin and P. Jeandet, *J. Phys. Chem. B*, 2005, **109**, 14573–14580.
- G. Liger-Belair, D. Topgaard, C. Voisin and P. Jeandet, *Langmuir*, 2004, **20**, 4132–4138.
- G. S. Barker, B. Jefferson and S. J. Judd, *Chem. Eng. Sci.*, 2002, **57**, 565–573.
- T. Cubaud, M. Sauzade and R. Sun, *Biomicrofluidics*, 2012, **6**, 022002.
- E. Tumarkin, Z. Nie, J. Il Park, M. Abolhasani, J. Greener, B. Sherwood-Lollar, A. Guenthere and E. Kumacheva, *Lab Chip*, 2011, **11**, 3545.
- A. Giacomello, M. Amabili and C. M. Casciola, *J. Phys.: Conf. Ser.*, 2015, **656**, 012124.
- Commercially available soap, Walch brand: fatty alcohol polyoxyethylene ether sodium sulfate 7%, cocamidopropyl betaine 7%, alkyl glycoside 2%, polyquaternium 0.1%, fatty glyceride 1.0%, humectant 3%, mixed plant extracts 1%, ethylenediamine tetraacetic acid tetrasodium salt 1%, sodium chloride 0.5%, citric acid 0.1%, jojoba oil 0.05%, 1,2-pentanediol 0.5%, essence 0.2%, water 76.55%.
- G. Liger-Belair, F. Sternenberg, S. Brunner, B. Robillard and C. Cilindre, *J. Food Eng.*, 2015, **163**, 60–70.
- X. Franka, N. Dietricha, J. Wub, R. Barrauda and H. Z. Lia, *Chem. Eng. Sci.*, 2007, **62**, 7090–7097.
- A. A. Solovev, S. Sanchez, Y. F. Mei and O. G. Schmidt, *Phys. Chem. Chem. Phys.*, 2011, **13**, 10131–10135.